13. Hiraide, M.; Ozaki, N.; Pak, Y. N.; Tanaka, T.; Kwaguchi, H. *Anal. Sci.* **1993**, *9*, 367.
14. Resing, J. A.; Mottle, M. J. *Anal. Chem.* **1992**, *64*, 2682.
15. Sakamoto-Arnold, C. M.; Johnson, K. S. *Anal. Chem.* **1987**, *59*, 1789.
16. Azeredo, L. C.; Sturgeon, R. E.; Curtius, A. *J. Spectrochim. Acta.* **1993**, *14B*(1), 91.
17. Mohammad, B.; Ure, A. M.; Littlejohn, D. *J. of Anal. Atom. Spectrom.* **1992**, *7*, 695.
18. Schuramel, P.; Xu, L. Q.; Knapp, G.; Michaelis, M. *Mikrochim. Acta.* **1992**, *106*, 191.
19. Sperling, M.; Xu, S.; Welz, B. *Anal. Chem.* **1992**, *64*, 3101.
20. Santelli, R. E.; Gallego, M.; Valcarcel, M. *Anal. Chem.* **1989**, *61*, 1427.
21. Welz, B.; Xu, S.; Sperling, M. *Appl. Spectrosc.* **1991**, *45*(9), 1433.
22. Fang, Z.; Dong, L. *J. of Anal. Atom. Spectrom.* **1992**, *7*, 439.
23. Zhuang, Z.; Wang, X.; Yang, P.; Yang, C.; Huang, B. *J. of Anal. Atom. Spectrom.* **1994**, *9*, 779.

Multidimensional Frictional Coupling Effect in the Photoisomerization of *trans*-Stilbene

Kijeong Kwac, Sangyoub Lee, and Kook Joe Shin*

Department of Chemistry, Seoul National University, Seoul 151-742, Korea
Received January 19, 1995

A model based on two coupled generalized Langevin equations is proposed to investigate the *trans*-stilbene photoisomerization dynamics. In this model, a system which has two independent coordinates is considered and these two system coordinates are coupled to the same harmonic bath. The direct coupling between the system coordinates is assumed negligible and these two coordinates influence each other through the frictional coupling mediated by solvent molecules. From the Hamiltonian which is equivalent to the coupled generalized Langevin equations, we obtain the transition state theory rate constants of the stilbene photoisomerization. The rates obtained from this model are compared to experimental results in *n*-alkane solvents.

Introduction

The photoisomerization of *trans*-stilbene has attracted considerable experimental[1~8] and theoretical[9~12] interests due to the fact that it provides a practical testing ground for theories of activated barrier crossing processes occurring in solution. In theoretical approaches to barrier crossing,[13~15] the dependence of reaction rate on solvent friction can be considered to have two phases. At very low friction the rate of energy accumulation in the reaction coordinate may be rate-limiting and the reaction rate will increase with increasing friction. At high friction regime the frictional effects resulting from multiple barrier crossing and recrossing begin to dominate and the reaction rate begins to decrease with increasing friction. Therefore a peak known as the Kramers turnover should exist in the variation of rate with friction. In the low viscosity regime there has been an effort to detect this maximum, and it has been only observed in pressurized gases but has not been observed in low viscosity liquid.[5,16]

The experimental situation of stilbene isomerization in alkane or alcohol solvent corresponds to high friction regime of Kramers theory. In this regime, there have been attempts to explain the effect of the medium on the isomerization rate in terms of the Kramers theory since Hochstrasser's initial application.[1,17] The Kramers theory is based on the concept of a Brownian particle escaping over a one-dimensional potential energy barrier along a potential energy curve that is piecewise parabolic. For the application to the *trans*-stilbene isomerization, the Kramers equation for the rate constant gives

$$k_{iso}=(\omega/2\pi)(\beta/2\omega')\{[1+(2\omega'/\beta)^2]^{1/2}-1\}\ e^{-E_b/kT} \quad (1)$$

where E_b is the barrier height, ω and ω' are the frequencies of the initial well and the curvature at the top of the barrier, respectively, and β is the reduced friction coefficient. Kramers' theory does not have the correct curvature necessary to describe the experimental results. It was found that the experimental results could be fitted very well to a viscosity dependence of the following form[2,3]

$$k_{iso}=\frac{A}{\eta^a}\exp(-E_b/kT) \quad (2)$$

where η is the solvent viscosity, A is a viscosity-independent constant, and the activation energy E_b is obtained by isoviscosity plots where the temperature is changed but the viscosity is held constant through the use of different solvents. The value of the empirical exponent a is typically between zero and unity.

Possible factors that result in the deviation from Kramers' theory are non-Markovian effects,[14,15,18] complicated interrelation between the microscopic friction and macroscopic visco-

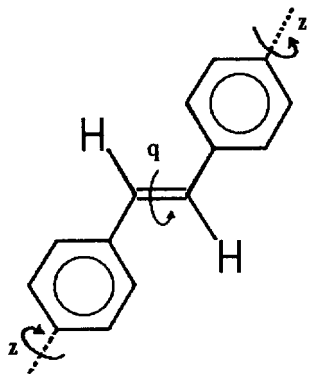

Figure 1. The system coordinates of *trans*-stilbene.

sity,[4] the solvent variation of barrier heights,[16] and the multidimensional nature of the reaction system,[9,19] etc. In particular, Agmon and Kosloff[9] have pointed out that if there is a transverse degree of freedom coupled strongly to the reaction coordinate dynamics, then the fractional dependence of rate on viscosity may arise.

In this paper we propose a model theory to treat the photoisomerization of *trans*-stilbene placing a focus on its multidimensional effects. The motion of *trans*-stilbene is composed of the internal rotation about the ethylenic bond (reaction coordinate, q) and the torsional motion around the bond joining the phenyl ring to the ethylenic carbon (perpendicular coordinate, z). Here for the phenyl ring torsion it is assumed that the two rings are moving with the same degree as shown in Figure 1. Multidimensional effect, or the influence of the phenyl ring torsions described by z coordinate on the rate of the isomerization described by q coordinate, is thought to stem from the frictional coupling between these two types of motion. That is, we assume that the dynamics of *trans*-stilbene can be described as a system with two independent coordinates which are coupled to the same bath of harmonic oscillators. In contrast to Agmon and Kosloff,[9] we neglect the direct coupling between the two reactant modes *via* any coupling potential. Instead, the modes are hydrodynamically coupled in an indirect way through the bath. Then we can construct two coupled generalized Langevin equations for the two system coordinates respectively and calculate the reaction rate through a normal mode analysis from the Hamiltonian which is equivalent to the coupled generalized Langevin equations (GLEs).[20,21]

This paper is organized as follows. In Sec. II, we describe the GLEs and corresponding Hamiltonian and derive the rate expression through a normal mode analysis. In Sec. III, we suggest a model of the frictional coupling and apply it to experimental results. Finally various aspects of this approach are discussed in Sec. IV.

Theory

A. Basic formalism. A system which has two independent modes is considered. As described in the introduction, the two system coordinates are coupled through frictional forces, and thus the equation of motion on each coordinate may be written as

$$M_q\ddot{q}+\frac{dV_1(q)}{dq}+M_q\int_0^t d\tau\gamma_q(t-\tau)\dot{q}(\tau)+(M_qM_z)^{1/2}\int_0^t d\tau\gamma_{qz}(t-\tau)\dot{z}(\tau)=\Gamma_q(t) \tag{3}$$

$$M_z\ddot{z}+\frac{dV_2(z)}{dz}+M_z\int_0^t d\tau\gamma_z(t-\tau)\dot{z}(\tau)+(M_qM_z)^{1/2}\int_0^t d\tau\gamma_{qz}(t-\tau)\dot{q}(\tau)=\Gamma_z(t) \tag{4}$$

where q and z are the system coordinates. And, $\gamma_q(t)$ and $\gamma_z(t)$ are the time-dependent friction acting upon q and z, respectively. $\Gamma_q(t)$ and $\Gamma_z(t)$ are fluctuating forces upon q and z coordinates. M_q and M_z are the effective masses associated with coordinates q and z moving in the potential field of $V_1(q)$ and $V_2(z)$, respectively. $\gamma_{qz}(t)$ represents the frictional coupling between the two system coordinates. These equations can be shown to be equivalent to the equation of motion derived from the Hamiltonian of the following form[20]

$$H=\frac{p_q^2}{2M_q}+\frac{p_z^2}{2M_z}+V(q,z)+\frac{1}{2}\sum_{j=1}^{N}\left[\frac{p_j^2}{m_j}+m_j\omega_j^2\left(x_j+\frac{c_{qj}q+c_{zj}z}{m_j\omega_j^2}\right)^2\right] \tag{5}$$

where (x_j, p_j) are the coordinates and conjugate momenta of the jth bath oscillator with mass m_j and frequency ω_j. The coefficients c_{qj} and c_{zj} couple the jth bath oscillator to the system coordinates q and z, respectively. The coupling between the two system coordinates in the potential energy surface is neglected. Thus,

$$V(q,z)=V_1(q)+V_2(z) \tag{6}$$

From the Hamiltonian of eq. (5), the equations of motion for the system (p_q, p_z, q, z) may be written exactly in the form of two coupled generalized Langevin equations under the following conditions. The time dependent friction is identified as

$$\gamma_q(t)=\sum_{j=1}^{N}\frac{c_{qj}^2}{M_qm_j\omega_j^2}\cos\omega_jt \tag{7}$$

$$\gamma_z(t)=\sum_{j=1}^{N}\frac{c_{zj}^2}{M_zm_j\omega_j^2}\cos\omega_jt \tag{8}$$

The Hamiltonian representation of the time dependent frictional coupling is

$$\gamma_{qz}(t)=\sum_{j=1}^{N}\frac{c_{qj}c_{zj}}{(M_qM_z)^{1/2}m_j\omega_j^2}\cos\omega_jt \tag{9}$$

The random forces are given in terms of the initial conditions of bath variables $(x_j(0), p_j(0))$ as

$$\Gamma_q(t)=-\sum_{j=1}^{N}c_{qj}\left\{\left[x_j(0)+\frac{c_{qj}}{m_j\omega_j^2}q(0)+\frac{c_{zj}}{m_j\omega_j^2}z(0)\right]\cos\omega_jt+\frac{p_j(0)}{m_j\omega_j}\sin\omega_jt\right\} \tag{10}$$

$$\Gamma_z(t)=-\sum_{j=1}^{N}c_{zj}\left\{\left[x_j(0)+\frac{c_{qj}}{m_j\omega_j^2}q(0)+\frac{c_{zj}}{m_j\omega_j^2}z(0)\right]\cos\omega_jt+\frac{p_j(0)}{m_j\omega_j}\sin\omega_jt\right\} \tag{11}$$

These two fluctuating forces $\Gamma_q(t)$ and $\Gamma_z(t)$ are Gaussian.[20] If one consider a bath that has equilibrated at $t=0$ in the presence of the system,[20] the appropriate initial bath distribution in phase space is given by

$$P[x(0),\ p(0)]=Z^{-1}e^{-H_B/kT} \tag{12}$$

where H_B is the bath Hamiltonian,

$$H_B=\sum_{i=1}^{N}\left[\frac{p_i^2}{2m_i}+m_i\omega_i^2\left(x_i+\frac{c_{qi}q+c_{zi}z}{m_i\omega_i^2}\right)^2\right] \tag{13}$$

With this distribution, the fluctuations $\Gamma_q(t)$ and $\Gamma_z(t)$ are zero centered:

$$<\Gamma_q(t)>=<\Gamma_z(t)>=0 \tag{14}$$

By direct calculation using eq. (12), we can obtain the fluctuation-dissipation relations[20] for each system coordinate

$$<\Gamma_q(t)\Gamma_q(\tau)>=kTM_q\gamma_q(t-\tau) \tag{15}$$

$$<\Gamma_z(t)\Gamma_z(\tau)>=kTM_z\gamma_z(t-\tau) \tag{16}$$

The correlation of the fluctuating forces $\Gamma_q(t)$, $\Gamma_z(t)$ is expressed explicitly as follows

$$<\Gamma_q(t)\Gamma_z(\tau)>=kT(M_qM_z)^{1/2}\ \gamma_{qz}(t-\tau) \tag{17}$$

If the right hand side does not vanish, the fluctuating forces on the q and z coordinates are correlated each other.

B. Normal Mode Analysis. Of the two system coordinates, q-coordinate is taken to be the reaction coordinate and z-coordinate a perpendicular coordinate. Along the reaction coordinate q, the potential is assumed to be harmonic and the barrier is located at $q=q^*$

$$V_1(q)=V^*-\frac{1}{2}M_q\omega_q^{*2}(q-q^*)^2 \tag{18}$$

Along the z-coordinate, the potential is given by

$$V_2(z)=\frac{1}{2}M_z\omega_z^{*2}z^2 \tag{19}$$

where ω_q^{*2} and ω_z^{*2} are curvatures along the reaction coordinate and the perpendicular direction, respectively, at $q=q^*$ on the potential energy surface and V^* is the height of the barrier. When we locate a well at $q=0$, the potentials along each coordinate are given by

$$V_1(q)=\frac{1}{2}M_q\omega_q^{o2}q^2 \tag{20}$$

$$V_2(z)=\frac{1}{2}M_z\omega_z^{o2}z^2 \tag{21}$$

where ω_q^{o2} and ω_z^{o2} represent curvatures along the reaction coordinate and in the perpendicular direction, respectively, at $q=0$ on the potential energy surface. In eqs. (19) and (21) the interaction of the two system modes can be taken into account implicitly to some extent by using different values of curvature, ω_z^{*2} and ω_z^{o2}.

Using the standard techniques,[21] we first transform to mass-weighted coordinates

$$q'=\sqrt{M_q}\,q,\ z'=\sqrt{M_z}\,z,\ x'_j=\sqrt{m_j}\,x_j \tag{22}$$

Then the Hamiltonian can be written as

$$H=\frac{p_{q'}^2}{2}+\frac{p_{z'}^2}{2}+V_1(q')+V_2(z')+\frac{1}{2}\sum_{j=1}^{N}\Big[p_{j'}^2+\omega_j^2x_j'^2+\frac{2c_{qj}}{\sqrt{M_qm_j}}q'x'_j+\frac{2c_{zj}}{\sqrt{M_zm_j}}z'x'_j+\frac{c_{qj}^2}{M_qm_j\omega_j^2}q'^2+\frac{c_{zj}^2}{M_zm_j\omega_j^2}z'^2+\frac{2c_{qj}c_{zj}}{m_j\omega_j^2\sqrt{M_qM_z}}q'z'\Big] \tag{23}$$

Diagonalizing the $(N+2)\times(N+2)$ force constant matrix $\boldsymbol{K}$ with respect to the mass-weighted coordinates, one can prove the following identities[21,22]

$$\det(\boldsymbol{K}^*)=-\lambda_o^{*2}\prod_{i=1}^{N+1}\lambda_i^{*2}=-\omega_q^{*2}\ \omega_z^{*2}\prod_{i=1}^{N}\omega_i^2 \tag{24}$$

$$\det(\boldsymbol{K}^o)=\lambda_o^{o2}\prod_{i=1}^{N+1}\lambda_i^{o2}=\omega_q^{o2}\ \omega_z^{o2}\prod_{i=1}^{N}\omega_i^2 \tag{25}$$

where $\boldsymbol{K}^o$ is the second order derivative matrix at the well and $\boldsymbol{K}^*$ at the barrier.

The transition state theory rate is given in terms of the product of all stable mode frequencies at the minimum and the inverse product of stable mode frequencies at the saddle point, respectively.[21] Using eqs. (24) and (25) we can write the rate as

$$k=\frac{\lambda_o^*}{2\pi}\frac{\omega_q^o\omega_z^o}{\omega_q^*\omega_z^*}\exp(-\beta E_b) \tag{26}$$

Using the relation

$$\det(\boldsymbol{K}^*-\lambda_o^{*2}\boldsymbol{I})=0, \tag{27}$$

we can express the positive-valued, unstable normal mode frequency λ_o^* in terms of the frictional kernel or its Laplace transform as

$$[\lambda_o^{*2}+\lambda_o^*\hat{\gamma}_q(\lambda_o^*)-\omega_q^{*2}][\lambda_o^{*2}+\lambda_o^*\hat{\gamma}_z(\lambda_o^*)+\omega_z^{*2}]-[\lambda_o^*\hat{\gamma}_{qz}(\lambda_o^*)]^2=0 \tag{28}$$

If we determine the explicit forms of the friction kernels for the system coordinates and the type of the frictional coupling, we can obtain the unstable mode frequencies as the largest positive solution of eq. (28) and calculate the rate using eq. (26).

Applications

A. Frictional Coupling. To apply the formalism described in the previous section to the photoisomerization of *trans*-stilbene, we should first construct a proper model of the frictional coupling which connects the two coordinates of the system. The Hamiltonian shown in Sec. II does not have any parameter which represents the explicit coupling between the two system coordinates, q and z, but the form of the Hamiltonian is made such that the mutual influence between q and z coordinates increases as the couplings between these and the bath coordinates increase. That is due to the fact that we neglect the direct coupling between the two system coordinates and assume only the existence of the indirect interaction through the bath oscillators.

The Hamiltonian representations of the friction kernels, eqs. (7)-(9), are multiplied by cos $\omega_j t$ and integrated over t to give

$$\int_0^\infty dt\gamma_q(t)\cos\omega_j t=\frac{\pi}{2M_q}\frac{c_{qj}^2}{m_j\omega_j^2} \tag{29}$$

$$\int_0^\infty dt\gamma_z(t)\cos\omega_j t=\frac{\pi}{2M_z}\frac{c_{zj}^2}{m_j\omega_j^2} \tag{30}$$

$$\int_0^\infty dt\gamma_{qz}(t)\cos\omega_j t=\frac{\pi}{2(M_qM_z)^{1/2}}\frac{c_{qj}c_{zj}}{m_j\omega_j^2} \tag{31}$$

Comparing these three equations, one can obtain

$$\left[\int_0^\infty dt\gamma_{qz}(t)\cos\omega_j t\right]^2=\left[\int_0^\infty dt\gamma_q(t)\cos\omega_j t\right]\left[\int_0^\infty dt\gamma_z(t)\cos\omega_j t\right] \tag{32}$$

In the continuum limit, integration in the bath frequency, ω, gives

$$\int_0^\infty d\omega\int_0^\infty dt\int_0^\infty dt'\gamma_{qz}(t)\ \gamma_{qz}(t')\cos\omega t\cos\omega t'$$
$$=\int_0^\infty d\omega\int_0^\infty dt\int_0^\infty dt'\gamma_q(t)\ \gamma_z(t')\cos\omega t\cos\omega t' \tag{33}$$

Using an identity[23]

$$\int_0^\infty d\omega\cos\omega t\cos\omega t'=\frac{\pi}{2}\delta(t-t') \tag{34}$$

we finally obtain

$$\int_0^\infty dt[\gamma_{qz}(t)]^2=\int_0^\infty dt\,\gamma_q(t)\gamma_z(t). \tag{35}$$

This is the relation between the friction kernels on the two system coordinates and the frictional coupling between them. This consequence means that eq. (35) is assumed implicitly when we write the coupled generalized Langevin equations as eqs. (3) and (4).

B. Application to Experimental Results. In the model proposed in the previous section the explicit forms of the time-dependent frictions are assumed to be exponential functions

$$\gamma_q(t)=\frac{\gamma_1}{\tau_1}\exp(-t/\tau_1) \tag{36}$$

$$\gamma_z(t)=\frac{\gamma_2}{\tau_2}\exp(-t/\tau_2) \tag{37}$$

$$\gamma_{qz}(t)=\frac{\gamma_c}{\tau_c}\exp(-t/\tau_c) \tag{38}$$

where γ is the friction coefficient and τ is the relaxation time of the medium. Substitution of these equations in eq. (35) gives the following result:

$$\frac{\gamma_c^2}{2\tau_c}=\frac{\gamma_1\gamma_2}{\tau_1+\tau_2} \tag{39}$$

From this relation we assume that the parameters for the frictional coupling are given by

$$\gamma_c^2=\gamma_1\gamma_2 \tag{40}$$

$$\tau_c=\frac{\tau_1+\tau_2}{2} \tag{41}$$

The relation between the friction coefficient and the solvent shear viscosity is given in the hydrodynamic model[24,12]

$$\gamma_1=\frac{6\pi\eta_s d^2}{M_q} \tag{42}$$

Table 1. Basic data for the *trans*-stilbene isomerization

d(Å)	r(Å)	$M_q\times10^{-45}$ kg·m²	$M_z\times10^{-45}$ kg·m²	$\omega_z^*\times10^{13}$ s^{-1}
3.7[a]	2.5[a]	4.33[b]	0.37[c]	0.898[d]

[a]Reference 1. [b]Reference 26. [c]Reference 19(b). [d]Reference 25.

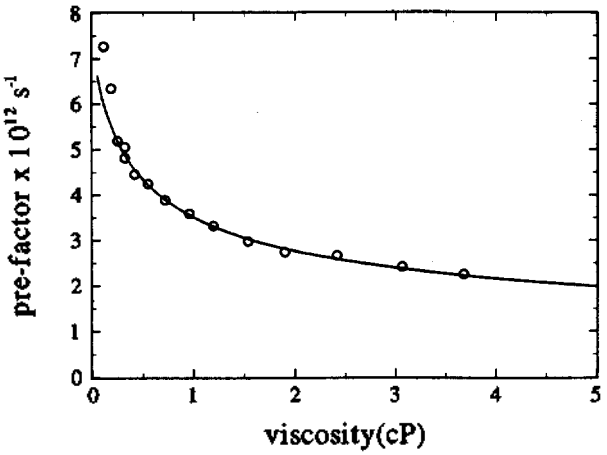

Figure 2. Plot of the reduced isomerization rate vs. the shear viscosity for stilbene in normal alkanes: ○ experimental results from ref. 1. — present model calculation.

$$\gamma_2=\frac{8\pi\eta_s d^3}{M_z} \tag{43}$$

where a stick boundary condition has been chosen and η_s is the solvent shear viscosity. M_q is a reduced moment of the rotation around the ethylenic bond and M_z for the torsion of the phenyl rings. d is the hydrodynamic radius of a sphere which corresponds to a phenyl ring and r is distance from the rotating axis. The values of these parameters used in the calculations are listed in Table 1.

To calculate the unstable mode frequency, λ_o^*, using eqs. (40) and (41), eq. (28) can be recast as follows

$$\left[\lambda_o^{*2}+\frac{\lambda_o^*\eta_1}{1+\lambda_o^*\tau_1}-\omega_q^{*2}\right]\left[\lambda_o^{*2}+\frac{\lambda_o^*\eta_2}{1+\lambda_o^*\tau_2}+\omega_o^{*2}\right]$$
$$-\frac{\lambda_o^{*2}\eta_1\eta_2}{[1+\lambda_o^*(\tau_1+\tau_2)/2]^2}=0 \tag{44}$$

To solve this equation for the unstable mode frequency, λ_o^*, we need to determine the curvatures of the potential energy surface of *trans*-stilbene at the barrier. For the value of the transverse mode frequency, ω_z^*, we use the estimate obtained by Spangler *et al.*[25] from spectroscopic data. The value is listed in Table 1. The value of ω_t^* is assumed to be the same as ω_z^*.

Hence there remain four adjustable parameters, τ_1, τ_2, ω_q^*, and ω_q^o, which are fitted to the experimental results. The fitted curve is shown in Figure 2 with experimental results for *trans*-stilbene in n-alkanes taken from Rothenberger *et al.*[1] The solid line in Figure 2 is obtained with the following parameter values: $\tau_1=0.10\times10^{-13}$ s, $\tau_2=3.45\times10^{-13}$ s, $\omega_q^*=0.57\times10^{13}$ s^{-1}, $\omega_q^o=4.9\times10^{13}$ s^{-1}.

Discussion

In this paper, we do not treat the solvent effect on the height of the potential energy barrier. Velsko *et al.*[27,28] showed that, for the cases of diphenylbutadiene in *n*-alkanes and the dye molecule, DODCI, in *n*-alkyl alcohols, the potential energy barrier effects could be separated from the dynamic solvent effect in the reactive process. This separation of static and dynamic solvent effects is not always possible.[28,29] But for the case of *trans*-stilbene in *n*-alkane solvent[1,2,7] it was possible to extract the activation energy from the slope of the isoviscosity plot. Hence in the present work only the pre-factor of the rate expression, eq. (26), is compared with the corresponding experimental results.[1] As shown in Figure 2, there is a good agreement between the model and the experimental data except in the low viscosity limit.

Of the four adjustable parameters, τ_1, τ_2, ω_q^*, and ω_q°, the three parameters, τ_1, τ_2, and ω_q^* determine the shape or curvature of the rate versus solvent viscosity curve. The reason is that in the pre-factor of the rate expression only the unstable mode frequency, λ_u^*, has the viscosity dependence and the relation used to obtain the unstable mode frequency, eq. (44), includes only these three parameters. ω_q° can change the absolute magnitude of the rate but not the shape of the curve.

The validity of eqs. (42) and (43) depends on the relative size of solvent and solute. In the experimental data used in Figure 1, the size of the solvent is changed when the viscosity is changed. As the size of solvent starts to exceed that of the solute, the validity of the hydrodynamic relations, eqs. (42) and (43), is rather ambiguous. There has been efforts to model the modified form of the friction in the one dimensional Kramers theory in order to consider the effect of solvent size.[4,31] But these efforts are not satisfactory. Treating the solvent size effect rigorously needs some microscopic theory and that is another problem. In this work, we take the exponential form as the friction and assume the form of hydrodynamic relation between the solvent viscosity and the friction coefficient. So, the quantities in eqs. (42) and (43) can be regarded as parameters adjusting the effect of solvent size to some extent.

From the result described in the previous section, the friction kernel for the reaction coordinate dynamics decays faster than that for the transverse mode. Unfortunately there is no experimental data to compare with. The calculated values of the relaxation times in both modes are very small. But we cannot say from this fact that the friction is time-independent in this formalism because the eqs. (36)-(38), (42) and (43) are very crude approximations. In order to clarify this point better, the friction kernel should be modeled by a more realistic form.

As mentioned by Spangler *et al.*[25] the frequency of phenyl ring torsion of *trans*-stilbene in the excited state is 47.7 cm^{-1} which is converted to 8.98×10^{12} s^{-1}. This transverse mode frequency is not expected to change much as going along the reaction coordinate from the well to the barrier region. Hence we use this value for both ω_z° and ω_z^*. The frequency of the ethylenic C-C torsion in *trans*-stilbene calculated by Warshel[30] was approximately 400 cm^{-1} which is converted to 7.5×10^{13} s^{-1}. This calculated value is comparable to the ω_q° value obtained in the present work. Note, however, that the ω_q^* value obtained is 0.57×10^{13} s^{-1} that is much smaller than ω_q°. This means that in the barrier region the curvature of potential energy surface along q becomes much smoother than in the well region. And this is the same conclusion as the previous one dimensional Kramers theory. The barrier frequency in the one dimensional Kramers theory with the frequency-dependent friction is 0.15×10^{13} s^{-1} by Rothenberger *et al.*[1] The barrier frequency in this work is roughly four times larger than that in the previous one dimensional Kramers theory. So we can say that when the transverse mode is taken into account the barrier become less smooth.

In this work, the coupling between q and z coordinates on the potential energy surface is ignored. But, as shown in eq. (5), the total Hamiltonian has the coupling term between q and z coordinates. The distinctive feature of this coupling term is that its strength is proportional to the strength of the interaction between these and the bath coordinates.

Acknowledgment. This work was supported by a grant (No. BSRI-93-311) from the Basic Science Research Institute Program, Ministry of Education of Korea, 1993.

References

1. Rothenberger, G.; Negus, D. K.; Hochstrasser, R. M. *J. Chem. Phys.* **1983**, *76*, 5360.
2. Courtney, S. H.; Flemming, G. R. *J. Chem. Phys.* **1985**, *83*, 215.
3. Kim, S. K.; Flemming, G. R. *J. Phys. Chem.* **1988**, *92*, 2168.
4. Lee, M.; Bain, A. J.; McCarthy, P. J.; Han, C. H.; Haseltine, J. N.; Smith II, A. B.; Hochstrasser, R. M. *J. Chem. Phys.* **1986**, *85*, 4341.
5. Schoeder, J. *Ber. Bunsenges. Phys. Chem.* **1991**, *95*, 233.
6. Schroeder, J.; Schwarzer, D.; Troe, J.; Voβ, F. *J. Chem. Phys.* **1990**, *93*, 2393.
7. Sundstroem, V.; Gillbro, T. *Ber. Bunsenges. Phys. Chem.* **1985**, *89*, 222, *Chem. Phys. Lett.* **1994**, *109*, 538.
8. Flemming, G. R.; Courtney, S. H.; Balk, M. W. *J. Stat. Phys.* **1986**, *42*, 83.
9. Agmon, N.; Kosloff, R. *J. Phys. Chem.* **1987**, *91*, 1988.
10. Kim, D.; Lee, S. *Bull. Korean Chem. Soc.* **1991**, *12*, 692.
11. Pollak, E. *J. Chem. Phys.* **1987**, *86*, 3944.
12. Sun, Y. P.; Saltiel, J. *J. Phys. Chem.* **1989**, *93*, 8310.
13. Kramers, H. A. *Physica* **1940**, *7*, 284.
14. Nitzan, A. *Adv. Chem. Phys.* **1988**, *70*, 489.
15. Hynes, J. T. in *Theory of Chemical Reaction Dynamics*; Bear, M. Eds.; Chemical Rubber: Boca Raton, FL, 1985; Vol. IV, p 171.
16. Troe, J. *J. Phys. Chem.* **1986**, *90*, 357.
17. Hochstrasser, R. M. *Pure Appl. Chem.* **1980**, *52*, 2683.
18. (a) R. F. Grote R. F.; Hynes, J. T. *J. Chem. Phys.* **1980**, *73*, 2715. (b) Grote, R. F.; van der Zwan, G.; Hynes, J. T. *J. Phys. Chem.* **1984**, *88*, 4676.
19. Park, N. S.; Waldeck, D. H. *J. Chem. Phys.* **1989**, *91*, 943, *Chem. Phys. Lett.* **1990**, *168*, 379.
20. E. Cortes, E.; West, B. J.; Lindenberg, K. *J. Chem. Phys.* **1985**, *82*, 2708.
21. Hanggi, P.; Talkner, P.; Borkevec, M. *Rev. Mod. Phys.* **1990**, *62*, 251.
22. Pollak, E. *J. Chem. Phys.* **1986**, *85*, 865.

23. Arfken, G. *Mathematical methods for physicists*; 2nd ed.; Academic Press: New York, 1970.
24. McCaskill, J. S.; Gillbert, R. G. *Chem. Phys.* **1979**, *44*, 389.
25. Spangler, L. H.; van Zee, R.; Zwier, T. S. *J. Phys. Chem.* **1987**, *91*, 2782.
26. Lee, J.; Zhu, S. B.; Robinson, G. W. *J. Phys. Chem.* **1987**, *91*, 4273.
27. Velsko, S. P.; Waldeck, D. H.; Fleming, G. R. *J. Chem. Phys.* **1983**, *78*, 249.
28. Zeglinski, D. M.; Waldeck, D. H. *J. Phys. Chem.* **1988**, *92*, 692.
29. Hicks, J. M.; Vandersall, M. T.; Sitzmann, E. V.; Eisenthal, K. B. *Chem. Phys. Lett.* **1987**, *135*, 413.
30. Warshel, A. *J. Chem. Phys.* **1975**, *62*, 214.
31. Dote, J. L.; Kivelson, D.; Schwartz, R. N. *J. Phys. Chem.* **1981**, *85*, 2169.

Thermodynamic Properties of Caffeine in Compressed Gas

Jeong Rim Kim and Jin Burm Kyong

Department of Chemistry, Hanyang University, Ansan 425-791, Korea
Received February 4, 1995

The solubility of caffeine in compressed carbon dioxide has been measured to determine its fugacity coefficient between 330 and 410 *K* up to 500 bar. The result allows the calculation of the thermodynamic excess functions such as the molar excess enthalpy, the molar excess free energy, and the molar excess entropy. The pressure variations of the molar excess functions of caffeine in the caffeine-CO_2 mixture were discussed and also compared them with those in the caffeine-NH_3 mixture.

Introduction

The solubility of a solid in a gas at law pressure is given by the vapor pressure of the solid. According to the Raoult's law and the Dalton's law, the following relationship holds for the solid component in the gaseous phase at low pressure.

$$y_2P=x_2P_2^o \tag{1}$$

where y_2 is the mole fraction of the solid component in the gaseous phase, x_2 in the solid phase, and P is the total pressure of the gaseous phase and P_2^o is the saturated vapor pressure of the solid component. Since we can assume that the mole fraction of gas in the solid phase is negligible at low pressure, the solubility of a solid in a gas is just the ratio of the vapor pressure to the total pressure. As the total pressure rises, equation (1) fails because of nonideal mixing in the gaseous phase which causes the fugacity of the solid component to be significantly different from its partial pressure. At higher pressures above the critical pressure of the gas, the nonideality of the gaseous phase becomes important in determining the solubility of the solid component.

There exist some partial data for the solubility of caffeine in carbon dioxide. They are the data up to 200 bar by Stahl and Schilz[1] and the data up to 160 bar by Ebeling and Franck.[2] There is also an equation for the solubility of caffeine in CO_2 in order to evaluate the interaction virial coefficients between caffeine and CO_2 by Lentz *et al.*[3] This work reports the data on the solubility of caffeine in compressed carbon dioxide between 330 K and 410 K up to 500 bar and uses them to determine the thermodynamic excess functions of caffeine due to mixing.

Thermodynamic Relationships

A binary system at temperature T and total pressure P consisting of caffeine as a heavy component 2 and carbon dioxide as a light component 1 will be considered in the present work. At equilibrium the distribution of the heavier component between the two phases of solid(S) and fluid(F) is governed by the Gibbs relation

$$f_2^S=f_2^F \tag{2}$$

The fugacity of caffeine (component 2) in the fluid phase is related to its mole fraction by

$$f_2^F=\varphi_2y_2P \tag{3}$$

where φ_2 is the fugacity coefficient of caffeine in the fluid phase and y_2 is its mole fraction. On the other hand, if the mole fraction of a gas in a solid is negligible compared with unity, then the solid phase is considered to be pure and the fugacity of caffeine in the solid phase is given by

$$f_2^S=P_2^o\varphi_2^o \exp\left[\int_{P_2^o}^{P}\frac{\bar{V}_2^S}{RT}\,dP\right] \tag{4}$$

where φ_2^o is the fugacity coefficient of the pure caffeine vapor and it is similar to unity because of the very low vapor pressure of pure caffeine. $\bar{V}_2^S$ is the molar volume of solid caffeine. Since we can assume $\bar{V}_2^S$ to be independent of pressure, equation (4) is rewritten